Available online at www.sciencedirect.com
SCIENCE DIRECT®
Surface Science 561 (2004) 248–260
SURFACE SCIENCE
www.elsevier.com/locate/susc

Adsorption sites of Te on Si(0 0 1)

P.F. Lyman [a,b,*], D.A. Walko [a,c], D.L. Marasco [a], H.L. Hutchason [a], M.E. Keeffe [a], P.A. Montano [d,e], M.J. Bedzyk [a,d,*]

[a] Department of Materials Science and Engineering, Northwestern University, Evanston, IL 60208, USA
[b] Department of Physics, University of Wisconsin-Milwaukee, Box 413, Milwaukee, WI 53201, USA
[c] MHATT-CAT, Advanced Photon Source, Argonne National Laboratory, Argonne, IL 60439, USA
[d] Materials Science Division, Argonne National Laboratory, Argonne, IL 60439, USA
[e] Department of Physics, University of Illinois at Chicago, Chicago, IL 60607, USA

Received 20 January 2004; accepted for publication 14 May 2004
Available online 31 May 2004

Abstract

Using multiple surface science techniques, we have investigated the structure of 0.3–1 Te monolayers adsorbed on Si(0 0 1). X-ray standing waves, low-energy electron diffraction, temperature-programmed desorption, and Auger electron spectroscopy show a relatively poorly-ordered surface. The disorder is due to two nearly degenerate Te adsorption sites, which tends to double the periodicity along one direction of the surface and reduces adatom/substrate mismatch by slightly increasing the separation of adjacent Te atoms. High-temperature anneals around 575 °C increase the degree of local and long-range order, while leaving the average local structure unchanged. Our findings are consistent with recent ab initio molecular dynamics simulations but not with experimental studies wherein surfaces were prepared by desorption of CdTe films.

Keywords: X-ray standing waves; Thermal desorption spectroscopy; Low energy electron diffraction (LEED); Surface structure, morphology, roughness, and topography; Silicon; Chalcogens; Low index single crystal surfaces

1. Introduction

Te on Si is an important surface system for issues of passivation [1,2], to improve growth of Ge films via surface-mediated epitaxy [3–6], and as a template for growth of CdTe films [7–9]. Despite the experimental and theoretical attention it has received, the Te/Si(0 0 1) surface structure remains controversial. While it is generally agreed that Te adsorbs in the bridge site as shown in Fig. 1a, a wide variety of low-energy electron diffraction (LEED) patterns have been reported, various X-ray photoelectron spectroscopy and scanning tunneling microscopy (STM) studies have reached conflicting interpretations, and wide variations in desorption temperatures have been measured. Some groups have proposed a surface structure of Te dimerization [10–12] or of a silicide formation [8,11], but these ideas remain controversial

* Corresponding authors. Address: Department of Materials Science and Engineering, Northwestern University, Evanston, IL 60208, USA. Tel.: +1-414-229-4626; fax: +1-414-229-5589.
E-mail addresses: plyman@uwm.edu (P.F. Lyman), bedzyk@northwestern.edu (M.J. Bedzyk).

0039-6028/$ - see front matter © 2004 Elsevier B.V. All rights reserved.
doi:10.1016/j.susc.2004.05.071

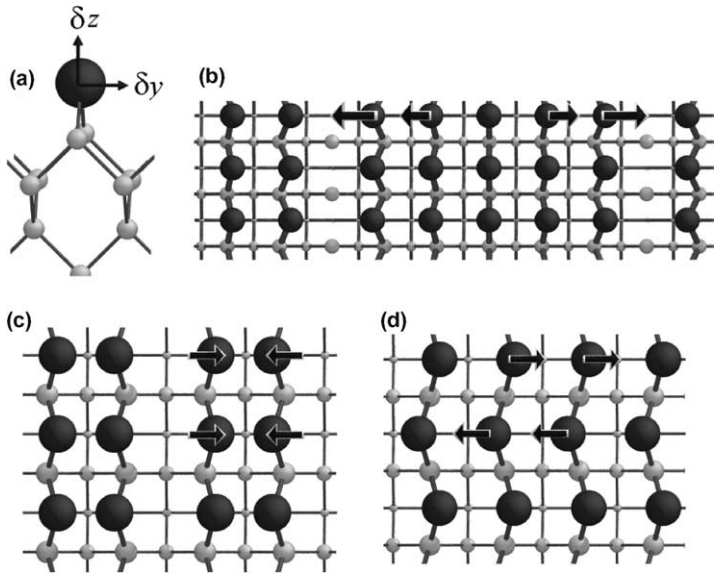

Fig. 1. (a) Bridge-site geometry for Te adsorbed on Si(0 0 1). Te atoms are larger and darker; Si atoms are lighter and decrease in size as one goes deeper into the bulk. δz and δy are the distances from the average absorption site to the actual position, in the [0 0 1] and [1 1 0] directions respectively. (b)–(d) Models of the structure of Te/Si(0 0 1), viewed from above. Arrows point in the directions in which Te is displaced from the ideal bridge site. (b) Missing-row model for the "streaky (1×1)" phase. (c) Two-site model with periodicity doubled in the y direction. (d) Two-site model with periodicity doubled in the x direction.

[2,13,14]. The wide variation in experimental results may be due in part to differences in sample preparation: some Te on Si(0 0 1) samples were prepared via deposition onto a clean substrate at room temperature, while others were prepared by growth of thick CdTe films followed by desorption of all but ~1 ML Te. Furthermore, the substrate temperature during Te deposition or post-growth annealing can critically affect the resulting surface phase, as we will show. Also, many of the past studies were limited to one or two primary methods of measurement, making it difficult to correlate results to those of other research groups. To gain better insight into the structure of Te on Si(0 0 1), we have approached the problem with several experimental techniques. By combining X-ray standing waves (XSW), temperature-programmed desorption (TPD), LEED, and Auger electron spectroscopy (AES) techniques, we have characterized the structure of Te/Si(0 0 1) as it evolves with annealing temperature. We find a relatively disordered surface with a number of metastable phases, thus explaining why so many apparently conflicting reports have been made.

2. Experiments

TPD experiments were performed in a custom ultra-high vacuum (UHV) chamber at Northwestern University, with a base pressure of $\sim3\times10^{-10}$ Torr. This chamber is equipped with standard surface science tools (LEED, AES, Knudsen cells for Te deposition) and a Stanford Research Systems RGA 300 residual gas analyzer (RGA). Substrate temperatures were measured with two infrared pyrometers, one optimized for low and one for high temperatures (below and above ~400 °C, respectively), and both calibrated ex situ with a thermocouple. P-doped Si(0 0 1) wafers, oriented to within ±0.25° of nominal, were used with direct-current heating. Samples were cleaned by heating to >1050 °C for 10 min., followed by a cooling rate of 1 °C/s. Tellurium was evaporated from a Knudsen cell operated at 350 °C onto the clean, room-temperature Si wafers for 10 min. Coverage was monitored qualitatively by AES. TPD spectra were acquired by monitoring the mass spectrometer partial pressure signal with time; Te_2 (whose signal was greatest at 256 amu)

was typically used because Te dimers are expected to be the species that desorbs. The Te_1 signal (greatest at 130 amu) was in fact significantly weaker than the Te_2 signal. An RGA cannot determine whether the Te_1 signal was due to desorbed Te monomers, doubly ionized dimers, or dimers that dissociated in the RGA field. Santucci et al. [13] hypothesized that, given the supposed strength of the adatom/substrate bond, the desorbing species would be TeSi, but the corresponding peak around 158 amu was never observed. A linear temperature ramp was maintained with a computer using SPEC [15] software macros to ramp the current through the sample, at heating rates $\beta = 0.5$–4°/s. The software controlled the ramp with a feedback loop using proportional and integrated controlling. Because the temperature profile was linear, temperature and time were easily calibrated, and the temperature could be directly related to the TPD spectra.

XSW experiments were conducted at beamline X15A of the National Synchrotron Light Source (NSLS), Brookhaven National Laboratory. The apparatus consists of several coupled UHV chambers (base pressure $\sim 9\times10^{-11}$ Torr) allowing sample preparation (molecular beam epitaxial growth) and characterization (LEED, AES, and XSW) in various subchambers. Temperatures were measured with either a pyrometer or thermocouple (for temperatures above or below 550 °C, respectively). A comprehensive review of the XSW technique and the experimental arrangement at X15A has been given by Zegenhagen [16].

For the X-ray measurements, the Si(0 0 1) samples were Syton-polished and chemically cleaned ex situ using the Shiraki process [17], and then mounted in a strain-free manner. After degassing each sample in UHV, the oxide was thermally desorbed at 900 °C. Upon cooling to room temperature (initial cooling rate ~2 °C/s), a sharp, two-domain (2×1) LEED pattern was observed. AES could detect no O and typically a small amount of C contamination (<0.02 ML). Te was deposited on the single crystal Si(0 0 1) substrates from an effusion cell at ~0.25 ML/min (1 ML $= 6.78\times10^{14}$ cm^{-2}). Most samples were prepared to a saturation coverage by exposure to ~3 ML of Te, often with the sample heated, while several other samples were prepared at subsaturation coverages by exposure to <1 ML Te. After initial measurements, some samples were further annealed to temperatures as high as $T_{sub} = 575$ °C for 10 min. Coverages were calibrated by the Te L fluorescence yield away from the Bragg condition and, for certain samples, by ex situ Rutherford backscattering analysis.

For XSW analysis, the incident X-ray beam from the synchrotron radiation source was collimated and monochromatized by a double-crystal monochromator and directed through a Be window into the UHV chamber. The sample, held at room temperature, was oriented to the 0 0 4 or the 0 2 2 diffraction planes in the Bragg reflection geometry, using 7.5-keV or 7.1-keV X-rays, respectively. Angular piezoelectric drives on both monochromator crystals were used to precisely scan through the several arcseconds-wide Bragg reflection. The resultant Te L fluorescence yield was detected by a energy-dispersive Si(Li) detector, while the reflected X-ray beam was measured by an in vacuo Si photodiode.

3. Experimental Results

3.1. Desorption kinetics and long-range order (TPD, AES, and LEED)

TPD experiments showed several distinct stages of Te desorption. For this set of experiments, several ML of Te were deposited on the clean Si(0 0 1)-(2×1) substrate at room temperature to saturation coverage. Immediately after Te deposition, no Si signal was visible in an AES scan, confirming a coverage of several ML. Shown in Fig. 2 is the Te_2 partial pressure as a function of temperature at $\beta = 2.0$°/s. The break in the spectrum around 400 °C is due to switching pyrometers. A surprisingly large number of peaks appear in these scans, compared to the relatively sparse TPD spectrum reported by Tamiya et al. [18]. The TPD data are analyzed according to the Redhead method [19] in Section (4.4). LEED patterns were also collected at various stages of annealing treatments. The LEED pattern of the as-deposited Te film, with no heat treatment, contained no

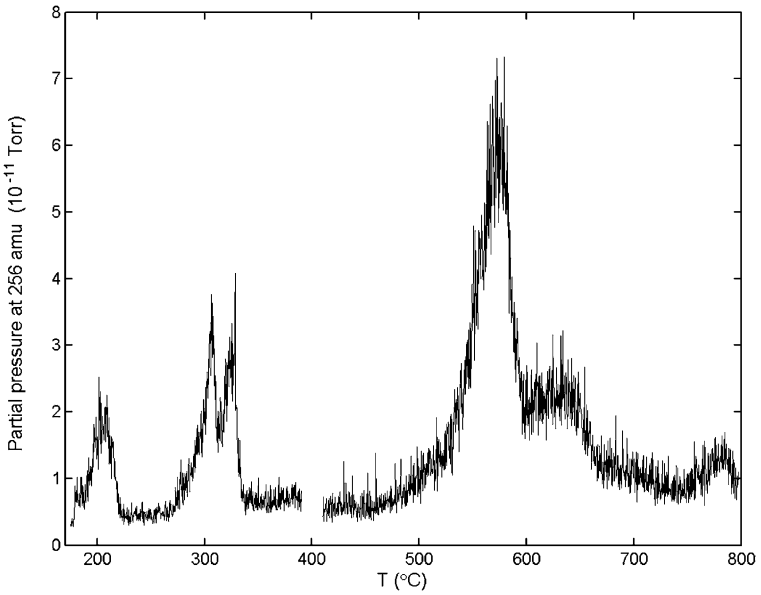

Fig. 2. Temperature-programmed desorption curves from Te/Si(0 0 1), ramped at $\beta = 2.°/s$. The scans were performed in two stages, with separate pyrometers used to collect data below and above 400 °C.

diffraction spots, only a diffuse background. Annealing to 250 °C resulted in a sharp (1×1) pattern (Fig. 3a) with no diffuse features. However, the LEED pattern after 350 °C displayed a (1×1) pattern with diffuse streaks in the [1 0] and [0 1] directions, as shown in Fig. 3b. We refer to this LEED pattern as "streaky (1×1)". After annealing to 570 °C, the LEED pattern changed

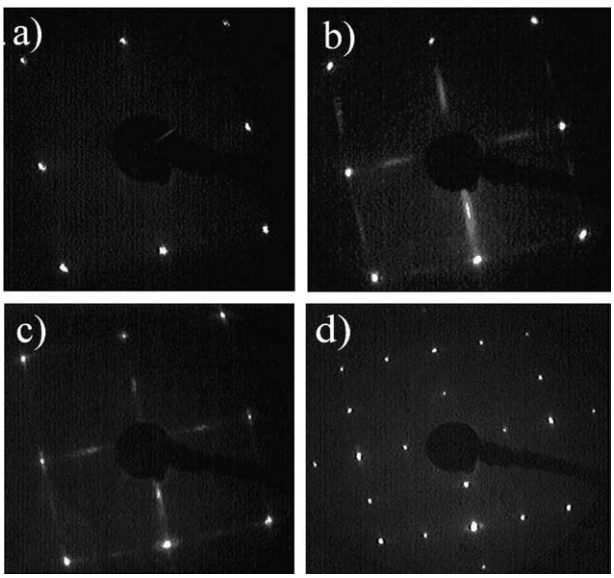

Fig. 3. LEED patterns from Te/Si(0 0 1): (a) (1×1) pattern after annealing at 250 °C; (b) "streaky (1×1)" pattern after annealing at 350 °C; (c) "streaky (2×1)" pattern after annealing at 570 °C and (d) clean (2×1) pattern after annealing at 690 °C.

further to a "streaky (2×1)" pattern, as seen in Fig. 3c, with half-order spots, again broadened in the [1 0] and [0 1] directions. As the temperature was increased, AES confirmed a decreasing Te/Si ratio; from the 350 °C anneal to the 570 °C anneal, the relative strength of the Te signal decreased by about 25%. Finally, the LEED pattern after 690 °C recovered the clean Si(0 0 1)-(2×1) pattern (Fig. 3d), with no Te observable by AES.

3.2. Local structure (XSW)

The XSW technique is a powerful probe of local structure, as it can overcome the classic "phase problem" of conventional crystallography. In the dynamical diffraction regime, incident and Bragg-diffracted X-rays coherently interfere, producing a standing-wave field in and above the crystal, with the XSW nodal planes parallel to and having the same periodicity as the diffraction planes. The phase of the standing wave with respect to the diffraction planes shifts by 180° as the Bragg angle θ is scanned from the low-angle side of the rocking curve to the high-angle side. This phase shift moves the antinodal planes of the standing wave inward by one-half of the lattice-plane spacing d_H. Thus, the angular dependence of the normalized fluorescence yield $Y(\theta)$ from an adatom layer can be described as

$$Y(\theta) = 1 + R(\theta) + 2\sqrt{R(\theta)} f_H \cos[v(\theta) - 2\pi P_H] \quad (1)$$

where $R(\theta)$ is the reflectivity and $v(\theta)$ is the relative phase between the incident and diffracted plane waves. The coherent fraction f_H and coherent position P_H correspond to the amplitude and phase, respectively, of the Hth Fourier component of the time-averaged spatial distribution of the adatoms (projected into a unit cell). H is the reciprocal lattice vector for the hkl diffraction planes, whose magnitude is defined as $2\pi/d_H$. Typically, the coherent fraction can be written as the product of three factors [20]:

$$f_H = C a_H D_H. \quad (2)$$

Here, C is the fraction of adatoms at ordered, or non-random, positions. D_H is the Debye–Waller factor

$$D_H = \exp\left(-2\pi^2 \langle u_H^2 \rangle / d_H^2\right), \quad (3)$$

where $\langle u_H^2 \rangle$ is the mean-squared displacement amplitude of the adatom projected in the H direction and d_H is the lattice-plane spacing. The Debye–Waller factor was originally derived for dynamic displacements due to thermal vibrations, but can also represent statically disordered atoms

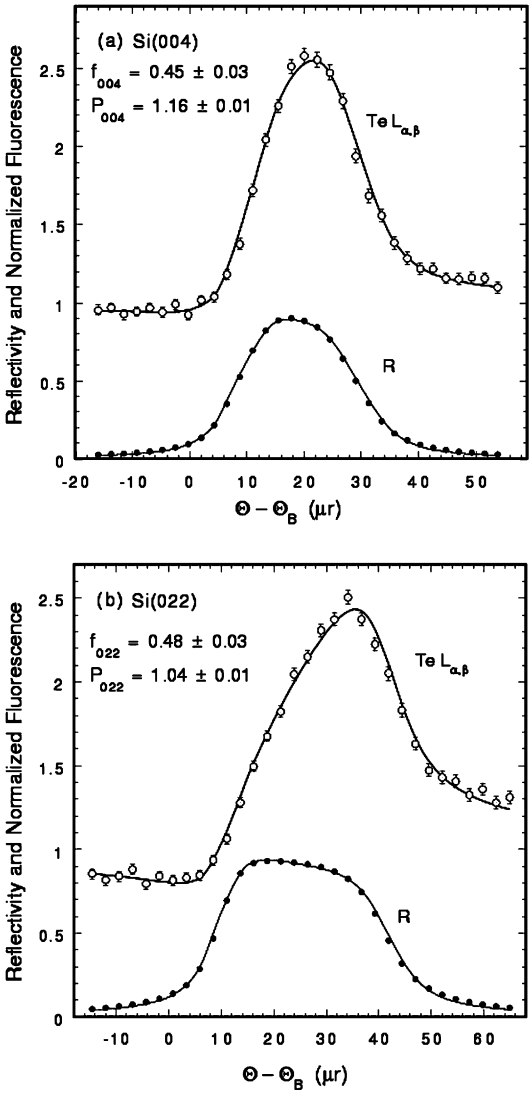

Fig. 4. XSW measurement of Te/Si(0 0 1) after anneals at low temperatures: X-ray reflectivity (R) and signal from the Te $L_{\alpha,\beta}$ fluorescence lines: (a) 0 0 4 reflection, with the lattice planes parallel to the surface; (b) off-normal 0 2 2 reflection.

displaced about an average location. Disorder due to multiple atomic positions is derived from the normalized geometric structure factor for ordered atoms, S_H. The magnitude of S_H is a_H, the geometrical factor in Eq. (2), while the phase of S_H is $2\pi P_H$. a_H describes the degree of uniformity of atomic positions and is given by

$$a_H = |S_H| = \left| \frac{1}{N} \sum_j^N \exp(\mathrm{i}H \cdot r_j) \right|. \quad (4)$$

The sum over j in Eq. (4) is for all N atomic positions located at well-defined fractional coordinates r_j of the bulk-extrapolated unit cell. In general, multiple well-defined atomic positions will result in values of a_H less than unity, while P_H can, in simple cases, be thought of as a weighted average of the ordered positions. We emphasize that the multiple atomic positions may be well-defined, but if they are distinct relative to the bulk diffraction planes, then the XSW technique interprets it as disorder. By performing "off-normal" XSW scans (i.e., diffraction vector H not parallel to the surface normal), then we can both triangulate the exact position of the adsorbate and investigate the lateral as well as vertical ordering.

XSW scans of Te/Si(0 0 1) samples annealed at low temperatures are shown in Fig. 4, with results for the 0 0 4 and 0 2 2 reflections in Figs. 4a and 4b, respectively. Fits to the XSW data yield coherent fractions and positions as summarized in Table 1. These XSW results, along with the "streaky (1×1)" LEED pattern, were consistently reproduced when depositing Te to saturation on a Si substrate heated to 200–270 °C, resulting in coverages of 0.3–0.9 ML, or after deposition at room temperature followed by annealing at 300 °C. Identical XSW results were also obtained upon depositing submonolayer coverages at 270 °C; in this case, the LEED patterns were a superposition of the "streaky (1×1)" pattern and sharp (2×1) spots. Presumably, this low-coverage surface is a mixture of Te-covered areas and clean, reconstructed Si.

In contrast, deposition at room temperature or 270 °C followed by annealing at 575 °C results in XSW scans as shown in Fig. 5. Compared to the lower-temperature results, the 0 0 4 and 0 2 2 coherent fractions rose almost 50% while the coherent positions remained essentially unchanged (see Table 1). Similar XSW results were also obtained when depositing Te directly onto Si heated at 475–575 °C, with resulting coverages from 0.6 to 0.9 ML. The corresponding LEED patterns are "streaky (2×1)," just as seen in the TPD experiments. Coverage measurements typically indicated that 575 °C anneals decreased the Te coverage by ~20%, but the exact coverage was apparently not a critical factor.

We note that an XSW measurement of the 0 0 4 reflection has previously been reported by Burgess et al. [21]. For a sample with a (1×1) LEED pattern, they reported a somewhat larger coherent position of $P_{004} = 1.20 \pm 0.02$ and a coherent fraction of $f_{004} = 0.65$. However, their sample was prepared by growth of a thick CdTe film followed

Table 1
Summary of experimental findings for the Te/Si(0 0 1) system, collected from over 20 individual XSW measurements

Preparation condition(s)	Observed coverages	LEED pattern	0 0 4 XSW	0 2 2 XSW
Deposit at room temp. (RT)	0.3–3	Diffuse	–	–
Deposit at RT then anneal at 250 °C	>1	1×1	–	–
Deposit at 200–270 °C or deposit at RT then anneal at 300 °C	0.3–1	Streaky 1×1	$f = 0.46$ $P = 1.15$	$f = 0.48$ $P = 1.04$
Deposit at or anneal to 475–575 °C	0.6–0.9	Streaky 2×1	$f = 0.68$ $P = 1.15$	$f = 0.66$ $P = 1.06$
Deposit <1 ML then anneal at 575 °C	~0.25	~2.5×1	$f = 0.64$ $P = 1.12$	$f = 0.64$ $P = 1.03$
Anneal to ~690 °C	0	Clean 2×1	–	–

Coverage is in monolayers (1 ML = 6.78×10^{14} cm^{-2}). The listed values of coherent fractions and coherent positions are averages of all relevant measurements; uncertainties are about ±0.02 for the coherent fractions and ±0.01 for the coherent positions.

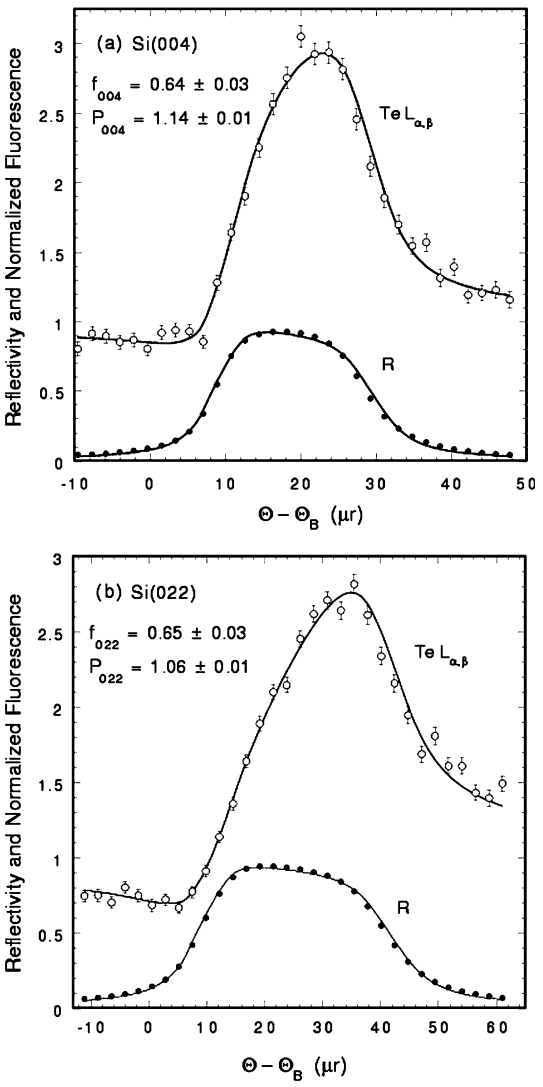

Fig. 5. XSW measurement of Te/Si(0 0 1) after annealing at high temperature: (a) 0 0 4 reflection and (b) 0 2 2 reflection.

by annealing, so their results may not be directly comparable to ours.

We observed one further adsorbate surface structure. Deposition of submonolayer amounts of Te followed by annealing at 575 °C for 5 min resulted in the LEED patterns with an "intermediate" superstructure between (2×1) and (3×1). Superstructure spots in the LEED pattern, although weak, were clearly visible about 0.4 of the way out of the Brillouin zone. The XSW results, shown in Table 1, were similar to the high-temperature, higher-coverage results except for small decreases in the 0 0 4 and 0 2 2 coherent positions. This implies that the local structure is not greatly changed even as the long-range order evolves (perhaps via the formation of domain walls, as proposed in Ref. [22]). Anneals to 690 °C always recovered the Si(0 0 1)-(2×1) surface, with fluorescence measurements yielding no signs of Te, thus confirming that Te does not diffuse into the bulk.

4. Te/Si(0 0 1) surface structures

4.1. Room-temperature surface structure

Before considering the possible structure of Te/Si(0 0 1) after annealing, we briefly discuss the structures formed after deposition of Te onto room-temperature Si(0 0 1). The lowest-temperature peak in the TPD spectra (Fig. 2) is identifiable as the desorption of all but ~1 ML of Te, as discussed below. The LEED pattern changes from diffuse, without any diffraction spots, to a sharp (1×1) pattern (Fig. 3a) reflecting the symmetry of the underlying Si. Such a sharp LEED pattern, without superstructure spots or significant diffuse streaking, has often been reported [3,6,13,18,23] for Te deposition at room temperature. We conclude that one ML of Te deposited at room temperature on Si corresponds to a metastable layer with limited ordering. While an XSW experiment was not performed on this surface, we expect XSW could not provide much useful information since the coherent fraction (see Eq. (2)) is likely quite low. A local-structure probe such as the Extended X-ray Absorption Fine Structure (EXAFS) technique could be used to characterize this surface by determining average bond lengths and coordination.

4.2. Structures of "streaky (1 × 1)" and "streaky (2 × 1)" phases

While several differences exist between our Te/Si(0 0 1) measurements after low-temperature and

after high-temperature anneals, the similarities are quite significant. First, we note that the 0 0 4 and 0 2 2 coherent positions remain, within uncertainty, unchanged between the two preparation conditions; that is, the average Te position remains constant. Second, the 0 0 4 and 0 2 2 coherent fractions both increase by ~40% from the low-temperature to the high-temperature anneal. Third, we have observed both structures over a range of coverages (as shown in Table 1), so neither phase requires special preparation conditions or a specific coverage such as 1/2 or 2/3 ML. And while the LEED pattern changes from "streaky (1×1)" to "streaky (2×1)," this could be interpreted not as a change in symmetry, but as a sharpening of a LEED pattern that was initially very diffuse. This difference in LEED patterns is not as significant as the qualitative change observed for Te/Ge(0 0 1), where the LEED pattern changes from streaky (1×1) to c(2×2) upon annealing at higher temperatures [24]. Indeed, in a series of LEED measurements, Ohtani et al. [22] noted that the streaky (1×1) to streaky (2×1) transition evolved continuously with temperature. Thus, the simplest description of the surface structure for <1 ML Te on Si(0 0 1) after anneals at 250–300 °C is that the structure is similar to, but less ordered than, the structure after anneals at 475–575 °C. In the context of the XSW coherent fraction (Eq. (2)), higher-temperature anneals increase C, the overall amount of Te in ordered sites, since the increase in the coherent fraction is not H-dependent. Changes to the geometrical structure or thermal vibration amplitude would not in general change f_{004} and f_{022} by the same factor; a_H and D_H depend, as the subscripts imply, on the scattering vector H. In the rest of this section, we analyze the Te/Si(0 0 1) surface structure by focusing on the better-ordered phase after high-temperature annealing, and present several models of the surface structure.

The XSW coherent positions of $P_{004} = 1.15$ and $P_{022} = 1.06$ are consistent with an atomic distribution centered on a twofold symmetry site, obeying (within error bars) the relation

$$P_{022} = \frac{1}{2}(1 + P_{004}). \tag{5}$$

The average Te height above the top Si plane is $P_{004} \cdot d_{004} = 1.56$ Å, implying that adsorption is at the bridge site, as expected from previous experimental [2,10,12,21,25] and theoretical [14,26,27] studies and shown in Fig. 1a. However, the coherent fractions are much less than expected for a highly ordered surface. A typical value of an adsorbate's vertical root-mean-square vibration amplitude for XSW measurements at room temperature is $\langle u^2_{004}\rangle^{1/2} = 0.14$ Å, as we previously determined for Te/Ge(0 0 1) and similar semiconductor/adsorbate systems [24]. The corresponding Debye–Waller portion of the coherent fraction would be $D_{004} = 0.9$, much higher than the measured coherent fractions. Thus, either the thermal vibration amplitude is much greater for Te on Si(0 0 1) than for comparable systems, or there is another form of "disorder." Referring again to Eq. (2), XSW "disorder" could be due to atomic thermal vibrations (D_H), atoms at multiple well-defined atomic sites (a_H), or atoms at ill-defined or random sites (C). Since the form or forms of disorder are never a priori known, one must create models to try to determine the structure. These models must be physically reasonable, following the constraints of the XSW data while being consistent with other available data, such as the symmetry of the observed LEED patterns.

The simplest possible model to interpret the XSW data assumes that the only disorder is due to thermal vibrations, i.e., $C = 1$ and $a_H = 1$. Since the Debye–Waller factors account for all of the disorder in this single-site model, the resulting vibration amplitudes are quite large: $\langle u^2_{004}\rangle^{1/2} = 0.19$ Å and $\langle u^2_{022}\rangle^{1/2} = 0.28$ Å. Note that the thermal vibrations are anisotropic even though the coherent fractions f_{004} and f_{022} are nearly equal; this is because the Debye–Waller factor D_H depends on the lattice-plane spacing (see Eq. (3)). As a modification to this model, one could assume a typical value [24] of 0.14 Å for $\langle u^2_{004}\rangle^{1/2}$, which yields a value of $C = 0.84$ (still assuming a single adsorption site, $a_H = 1$). The off-normal thermal vibration amplitude is then $\langle u^2_{022}\rangle^{1/2} = 0.21$ Å. If either single-site model is correct, then Te/Si(0 0 1) exhibits the unusual, but not unique, situation of adatoms having larger thermal vibrations in the plane of the surface than perpendicular to the

surface. However, any single-site model fails to qualitatively explain the "streaky (2×1)" LEED pattern. Thus, a model with a distribution of Te positions, i.e., $a_H < 1$, is needed.

One model that incorporates multiple Te positions was first suggested by Yoshikawa et al. [25]. In an STM experiment, they observed regions of (1×1) structure interrupted by Te-free rows, shown schematically in Fig. 1b. These missing rows were thought to relieve the compressive stress of large adatoms on the Si substrate. The Te atoms then can relax laterally towards the missing rows. With every sixth or seventh Te row missing, such a structure was consistent with the measured coverage (~0.8 ML) and a streaky (1×1) LEED pattern (since the missing rows create a type of superstructure, but lack a well-defined length scale). In fact, this structure was the best model for our previous XSW measurements of Te/Ge(0 0 1) after low-temperature annealing, which had a similarly streaky (1×1) LEED pattern [24]. However, we note that the coherent fractions measured for Te/Ge(0 0 1) (Ref. [24]) were significantly larger than the present case of Te/Si(0 0 1). The Te on Si system is thus more disordered, which is consistent with disorder caused by adatom/substrate size mismatch. If one assumes isotropic displacement amplitudes of $\langle u^2_{004}\rangle^{1/2} = \langle u^2_{022}\rangle^{1/2} = 0.15$ Å, then $C = 0.58$, using the XSW results from the streaky (1×1) surface. Compared to atoms at the ideal bridge site, the average Te–Te spacing increases by 3–5% depending on whether the model assumes a uniform Te–Si bond length or a uniform height of Te above the surface. However, this model cannot be reconciled with the streaky (2×1) surface since the model provides no source of twofold periodicity. If, as we argued above, the streaky (1×1) to streaky (2×1) transformation is simply an increase in order rather than a qualitative structural change, then another model must be found.

For a more satisfactory model of Te/Si(0 0 1), we propose that the adatoms are centered on the bridge sites, but the adsorption site is split vertically and/or horizontally. Variations on this model have been considered by several groups [10,12,21, 26,28]. For example, one can model of the structure as adatoms at one vertical position ($\delta z = 0$, as defined in Fig. 1a) but two lateral positions. If one assumes $\langle u^2_{004}\rangle^{1/2} = \langle u^2_{022}\rangle^{1/2} = 0.15$ Å, then the XSW measurements constrain the lateral adsorption site to be offset $\delta y = 0.33$ Å from the average position; in this example $C = 0.86$. Alternately, the two adsorption sites could be split vertically as well as laterally. If one now assumes a fully ordered structure ($C = 1$), again with an isotropic Debye–Waller factor ($\langle u^2_{004}\rangle^{1/2} = \langle u^2_{022}\rangle^{1/2} = 0.15$ Å), then the site splitting is $\delta y = 0.43$ Å and $\delta z = 0.11$ Å. Such a model, with vertical rippling of the adatoms, may result in two significantly different Te–Si bond lengths unless atoms in the top Si layer are significantly moved from their bulk-like positions. Lacking clear experimental evidence for rippling or for multiple Te–Si bond lengths, we conclude that the two-site model, with lateral but not vertical splitting of the Te sites, best describes the Te/Si(0 0 1) surface structure. Of course, with XSW measurements at only two reflections, this model is underdetermined, and the details of this model depend on parameters such as the assumed values of the thermal vibration amplitudes.

The two-site model we propose is compatible with (2×1) symmetry if Te adatoms in adjacent sites are displaced in alternating directions. Taking the model of laterally split Te sites, if a given atom is displaced by $+\delta y$, its neighbors along the direction in which periodicity is doubled will be displaced by $-\delta y$, while its neighbors in the other direction will be displaced by $+\delta y$. If the period is doubled along the y direction (as shown in Fig. 1c), then some Te atoms will grow closer together than Te atoms at ideal bridge sites. For $+\delta y = 0.33$ Å, this model yields a Te–Te interatomic separation of 3.18 Å. While some experiments have proposed model structures involving Te_2 dimers, in some cases with vertical rippling [10–12], dimerization contradicts the expected bonding of divalent Te and is unsupported by theoretical calculations [14,27]. We note that all experiments that suggest dimer formation [10–12] were performed with growth of CdTe films or by desorbing thick CdTe films to recover a Te/Si(0 0 1) surface; the presence of Cd may alter the surface structure or complicate the data interpretation. Much more likely for the Te/Si(0 0 1) system without Cd is an increase in the Te–Te separation, due to doubling the period

along the x direction, as shown in Fig. 1d. This would tend to relieve the strain of large adatoms on a small substrate; the Te–Te separation increases to 3.9 Å in the x direction. This is supported by the series of LEED patterns vs. temperature obtained by Tamiya et al. [18] on a single-domain surface. They found that the LEED spots from clean Si(0 0 1) were rotated 90° from the streaky (2×1) spots due to ~1 ML Te. Such structures are consistent with calculations by Sen et al. [27], who performed ab initio molecular dynamics (MD) simulations at 330 and 730 °C. The high-temperature MD simulations, performed for a (4×1) supercell, showed very large vibrational amplitudes in the z and y directions (as defined in Fig. 1) due to soft phonons in the "easy" y direction. But calculations of the adatoms' potential well at $T = 0$ K showed a very wide, anharmonic well in the y direction; if alternating Te were displaced in opposite directions then a double-well structure was found with $\delta y \sim 0.25$ Å. Unfortunately, a direct comparison with experiments conducted at room-temperature is not possible since the MD simulations were carried out at elevated temperatures, where no stable (2×1) phase was found. On the other hand, total-energy calculations by Takeuchi [26] found a spontaneous period doubling by lateral relaxations of the Te at 1 ML coverage. Takeuchi found that a variety of similar configurations had similar total energies, which easily led to disorder and an interruption of the (2×1) symmetry, and thus the streakiness of the LEED patterns. Neither Sen et al. nor Takeuchi explicitly reported vertical rippling of Te at 1 ML coverage, but no such rippling was found in the density functional theory calculations of Miwa and Ferraz [14].

4.3. Structure of "intermediate superstructure" phase

Finally, we remark on the surface whose LEED pattern roughly indexes as $(\frac{5}{2}\times1)$. A similar LEED pattern for Te/Si was observed by Ohtani et al. [22], who, in a systematic study of LEED patterns vs. annealing temperature, found a wide range of intermediate patterns between (1×1) and (2×1) at successive anneals from 400 to 650 °C, then from (1×3) to clean (1×2) for anneals from 680 to 720 °C. Ohtani et al. interpreted the results as evidence for domain wall formation. A similar experiment was not practical in our vacuum system, where sample preparation, LEED measurements, and XSW measurements are performed in separate subchambers. We suppose the reconstructions such as the reported (3×1) and (1×2) correspond to special coverages which we did not happen to obtain in this preparation (submonolayer deposition followed by a 12 min anneal at 300 °C and a 5 min anneal at 575 °C); such structures have been investigated theoretically by Miwa et al. [14]. Nevertheless, our XSW measurements reveal that as the domain walls begin to form, the average Te position slightly shifts inwards. The 0 0 4 and 0 2 2 coherent positions both decrease, with the adatoms shifting toward the surface by 0.04 Å. The relative values of P_{004} and P_{022} may indicate a shift away from the bridge site (since the measured positions do not quite satisfy Eq. (5)). It is possible that the reconstruction occurs by some fraction of the Te atoms shifting to a lower site as a domain wall is formed, while the rest remain at their original position. XSW measurements at a variety of coverages, including the integer reconstructions such as (3×1), would help in constructing structural models for such domain-wall surfaces.

4.4. Te binding energies for various phases

Having determined the evolution of Te/Si(0 0 1) surface structures with annealing, we now analyze the TPD data presented in Section 3.1 to determine the desorption energy E_d at the various stages of desorption. Having measured T_p, the temperature of the peak desorption rate at various heating rates β, we follow Falconer and Madix [29] in writing the Redhead equation [19] as

$$\ln(\beta/T_p^2) = \ln(Rvc^{n-1}/E_d) - E_d/RT_p. \quad (6)$$

Here, R is the molar gas constant, n is the order of the reaction, v is the pre-exponential factor, and c is the initial coverage. An Arrhenius-type plot yields E_d from the slope and v from the intercept. This method avoids the danger of assuming a

particular value for ν, but assumes that ν is independent of E_d and that both ν and E_d are independent of coverage. In fact, we find in the analyses below that ν is significantly less than the canonical value of 10^{13} s^{-1}. But since ν is found by extrapolation (and after assumption of an initial coverage, for second-order desorption), our resulting values of $\nu \sim 10^{7-11}$ s^{-1} are not very reliable.

The first peaks in the TPD scans (Fig. 2) occurred at $T_p \approx 200$ °C. The shapes of these peaks were generally asymmetric, indicative of a first-order reaction [19]. First-order kinetics may seem surprising at first glance, given that Te desorbs as dimers. But at coverages of several ML, desorption is apparently not rate-limited by dimerization of the desorbing species. This peak corresponds to desorption of the weakly bound Te overlayers, with the surface coverage decreasing from saturation (~3 ML) to probably about 1 ML as proposed previously [1,18]; analysis according to Eq. (6) yields a value of $E_d = 0.7$ eV.

The next set of reproducible peaks in the TPD spectra occurred in the region of $T_p \approx 325$ °C, but there were often other peaks at somewhat lower temperatures (260–310 °C). Both peaks are asymmetric and thus first-order, as shown in Fig. 2. The higher-temperature peaks can be identified with the phase transition in which the LEED pattern changes from plain (1×1) to streaky (1×1) and analysis yields $E_d = 1.3$ eV. The other peaks at slightly lower T_p vary drastically among the various TPD scans and cannot be analyzed by Eq. (6). These peaks appear to be highly preparation-dependent, possibly determined by the Te coverage at the start of the TPD scan.

At higher temperatures, there are large peaks in the TPD spectra around 560 °C. These are naturally interpreted as the transition from the streaky (1×1) to streaky (2×1) phase. These symmetric peaks imply second-order kinetics [19] with $E_d = 1.9$ eV. However, most scans exhibited shoulders and/or smaller peaks on the high-temperature side of the main peak. These features correspond to desorption as the domain walls [22] evolve. The positions of these smaller peaks vary widely from scan to scan and probably depend sensitively on the exact Te coverage and detailed structure of the surface; as such, they are not amenable to interpretation via Eq. (6). At still higher temperatures is the final peak around 760 °C, which corresponds to complete desorption of Te from the surface and has $E_d = 2.6$ eV.

5. Conclusion

The results of this investigation reveal an unusual adsorption situation for Te, with two nearly degenerate adsorption sites split by a small distance. The missing-row model appears to satisfactorily account for the streaky (1×1) phase, but does not describe the streaky (2×1) phase. Missing rows may still exist on Te/Si(0 0 1) to relieve strain, but they are not the primary feature of the surface structure, as they are for Te/Ge(0 0 1)-(1×1). Our limited XSW data set cannot determine with certainty whether the splitting in the proposed two-site model is vertical, lateral, or a combination of the two, nor if there are other forms of disorder such as anomalously large thermal vibration amplitudes. This ambiguity can be cleared up by XSW measurements of higher-order reflections such as 0 4 4 or 0 0 8, which, because of smaller lattice-plane spacing, provide higher positional sensitivity and are more sensitive to disorder. Additionally, the Fourier summation of a more complete set of XSW amplitudes f_H and phases P_H could produce a model-independent image of the Te atom distribution, as has recently been demonstrated for other adsorbate systems [30,31]. A model-independent structural solution avoids the need to separate the sources of "disorder" into three distinct components (see Eq. (2)). Given a highly anharmonic potential well [28], wherein the positional splitting is of the same order as the thermal vibrational amplitude, the distinction becomes somewhat artificial.

Performing XSW and LEED measurements below room temperature may determine whether Te does form any stable, highly ordered reconstructions on Si(0 0 1). Lowering the temperature would reduce the thermal vibration amplitude, lessening the effect of the Debye–Waller factor on the coherent fraction and thus making the measurement more sensitive to the geometrical factor a_H. Lower temperatures would also, of course, re-

duce any effect that thermal vibrations might have in limiting the long-range order as reflected by the streakiness of the LEED patterns. Such measurements were not feasible in our UHV chamber at NSLS, but could be done at a third-generation source such as the Advanced Photon Source in a chamber with a variable-temperature sample stage. Investigations of the higher-order reconstructions, presumably due to domain-wall formation [22], would also be easier in a UHV system where sample heating and measurement could be done without transferring the sample between chambers.

Even as the structural details of the two-site adsorption model become clear, its origin, and even more so its temperature dependence, remain intriguing. The splitting of the adsorption site is most likely due to a strain-driven instability due to adsorbate/substrate mismatch. Intuitively, the size mismatch of large Te adatoms on the smaller Si lattice is an attractive explanation of the site splitting, but detailed calculations which take into account the constraints provided by the present XSW data are needed to quantify this. Further investigations are needed to determine the mechanism by which high-temperature anneals (around 575 °C) increase the local and long-range ordering of the adsorbate (as measured by increased XSW coherent fraction and decreased LEED streakiness, respectively). Such studies will be complicated by the apparently metastable phases which, based on their highly variable peaks in the TPD spectra, appear to be highly preparation-dependent, such as the domain-wall evolution. A further complication appears to be that experimental results tend to differ, depending on whether the surface was prepared by growing and then desorbing thick CdTe films.

Acknowledgements

We wish to thank T.-L. Lee for help with the TPD experiment and P. Sen for helpful discussions. This work was supported by the US Department of Energy under contract No. W-31-109-ENG-38 to Argonne National Laboratory, contract No. DE-AC02-98CH10886 to National Synchrotron Light Source at Brookhaven National Laboratory, and by the National Science Foundation under contract No. DMR-9973436, and under contract No. DMR-0076097 to the MRC at Northwestern University. One of us (PFL) is supported by NSF Grant No. DMR-9984442.

References

[1] S. Di Nardo, L. Lozzi, M. Passacantando, P. Picozzi, S. Santucci, J. Elec. Spectr. Rel. Phenom. 74 (1995) 129.
[2] M.R. Bennett, A.A. Cafolla, J.W. Cairns, C.J. Dunscombe, R.H. Williams, Surf. Sci. 360 (1996) 187.
[3] S. Higuchi, Y. Nakanishi, Surf. Sci. 254 (1991) L465.
[4] H.J. Osten, J. Klatt, G. Lippert, E. Bugiel, S. Higuchi, J. Appl. Phys. 74 (1993) 2507.
[5] X. Yang, R. Cao, J. Li, J. Terry, J. Wu, P. Pianetta, in: P. Fuoss et al. (Ed.), Material Research Society Symposium Proceedings, vol. 312, Materials Research Society, 1993, p. 243.
[6] M.R. Bennett, C.J. Dunscombe, A.A. Cafolla, J.W. Cairns, J.E. Macdonald, R.H. Williams, Surf. Sci. 380 (1997) 178.
[7] I. Sugiyama, Y. Nishijima, Appl. Phys. Lett. 66 (1995) 2798.
[8] D.J. Wallis, N.D. Browning, S. Sivananthan, P.D. Nellist, S.J. Pennycook, Appl. Phys. Lett. 70 (1997) 3113.
[9] Y. Xin, N.D. Browning, S. Rujirawat, S. Sivananthan, Y.P. Chen, P.D. Nellist, S.J. Pennycook, J. Appl. Phys. 84 (1998) 4292.
[10] F. Wiame, G. Mathot, S. Sivananthan, S. Rujirawat, R. Caudano, R. Sporken, Appl. Surf. Sci. 142 (1999) 475.
[11] R. Sporken, F. Malengreau, J. Ghijsen, R. Caudano, S. Sivananthan, J.P. Faurie, T. van Gemmeren, R.L. Johnson, Appl. Surf. Sci. 123/124 (1998) 462.
[12] H.S. Jung, H.J. Kim, Curr. Appl. Phys. 2 (2002) 389.
[13] S. Santucci, S. Di Nardo, L. Lozzi, M. Passacantando, P. Picozzi, Surf. Sci. 352–354 (1996) 1027.
[14] R.H. Miwa, A.C. Ferraz, Surf. Sci. 449 (2000) 180.
[15] Certified Scientific Software, Cambridge, MA.
[16] J. Zegenhagen, Surf. Sci. Rep. 18 (1993) 199.
[17] A. Ishizaka, Y. Shiraki, J. Electrochem. Soc. 133 (1986) 666.
[18] K. Tamiya, T. Ohtani, Y. Takeda, T. Urano, S. Hongo, Surf. Sci. 408 (1998) 268.
[19] P.A. Redhead, Vacuum 12 (1962) 203.
[20] M.J. Bedzyk, L. Cheng, in: P. Fenter, M. Rivers, N.C. Sturchio, S. Sutton (Eds.), Reviews in Minerology and Geochemistry, vol. 49, Geochemical Society, 2002, p. 221.
[21] S.R. Burgess, B.C.C. Cowie, S.P. Wilks, P.R. Dunstan, C.J. Dunscombe, R.H. Williams, Appl. Surf. Sci. 104/105 (1996) 152.
[22] T. Ohtani, K. Tamiya, Y. Takeda, T. Urano, S. Hongo, Appl. Surf. Sci. 130–132 (1998) 112.

[23] S. Di Nardo, L. Lozzi, M. Passacantando, P. Picozzi, S. Santucci, Surf. Sci. 331–333 (1995) 569.
[24] P.F. Lyman, D.L. Marasco, D.A. Walko, M.J. Bedzyk, Phys. Rev. B 60 (1999) 8704.
[25] S.A. Yoshikawa, J. Nogami, C.F. Quate, P. Pianetta, Surf. Sci. 321 (1994) L183.
[26] N. Takeuchi, Phys. Rev. B 60 (1999) 4796.
[27] P. Sen, S. Ciraci, I.P. Batra, C.H. Grein, Phys. Rev. B 64 (2001) 193310.
[28] P. Sen, S. Ciraci, I.P. Batra, C.H. Grein, S. Sivananthan, Surf. Sci. 519 (2002) 79.
[29] J.L. Falconer, R.J. Madix, Surf. Sci. 48 (1975) 393.
[30] J.S. Okasinski, C.-Y. Kim, D.A. Walko, M.J. Bedzyk, Phys. Rev. B 69 (2004) 041401.
[31] Z. Zhang, P. Fenter, L. Cheng, N.C. Sturchio, M.J. Bedzyk, M.L. Machesky, D.J. Wesolowski, Surf. Sci. 554 (2004) L95.